The Journal of Experimental Biology 207, 1953-1967
Published by The Company of Biologists 2004
doi:10.1242/jeb.00993

Swimming gaits, passive drag and buoyancy of diving sperm whales *Physeter macrocephalus*

Patrick J. O. Miller[1,2,*], Mark P. Johnson[3], Peter L. Tyack[2], Eugene A. Terray[3]

[1]*Sea Mammal Research Unit, University of St Andrews, Fife, KY16 8LB, Scotland*, [2]*Biology Department* and [3]*Department of Applied Ocean Physics and Engineering, Woods Hole Oceanographic Institution, Woods Hole, MA 02543, USA*

*Author for correspondence at address 1 (e-mail: pm29@st-and.ac.uk)

Accepted 22 March 2004

Summary

Drag and buoyancy are two primary external forces acting on diving marine mammals. The strength of these forces modulates the energetic cost of movement and may influence swimming style (gait). Here we use a high-resolution digital tag to record depth, 3-D orientation, and sounds heard and produced by 23 deep-diving sperm whales in the Ligurian Sea and Gulf of Mexico. Periods of active thrusting *versus* gliding were identified through analysis of oscillations measured by a 3-axis accelerometer. Accelerations during 382 ascent glides of five whales (which made two or more steep ascents and for which we obtained a measurement of length) were strongly affected by depth and speed at Reynold's numbers of 1.4–2.8×10^7. The accelerations fit a model of drag, air buoyancy and tissue buoyancy forces with an r^2 of 99.1–99.8% for each whale. The model provided estimates (mean ± S.D.) of the drag coefficient (0.00306±0.00015), air carried from the surface (26.4±3.9 l kg^{-3} mass), and tissue density (1030±0.8 kg m^{-3}) of these five animals. The model predicts strong positive buoyancy forces in the top 100 m of the water column, decreasing to near neutral buoyancy at 250–850 m. Mean descent speeds (1.45±0.19 m s^{-1}) were slower than ascent speeds (1.63±0.22 m s^{-1}), even though sperm whales stroked steadily (glides 5.3±6.3%) throughout descents and employed predominantly stroke-and-glide swimming (glides 37.7±16.4%) during ascents. Whales glided more during portions of dives when buoyancy aided their movement, and whales that glided more during ascent glided less during descent (and *vice versa*), supporting the hypothesis that buoyancy influences behavioural swimming decisions. One whale rested at ~10 m depth for more than 10 min without fluking, regulating its buoyancy by releasing air bubbles.

Key words: drag, buoyancy, sperm whale, *Physeter macrocephalus*, swimming gait, diving.

Introduction

External forces that act on moving animals are important in their life history because such forces affect the energetic cost of movement, generally termed 'cost-of-transportation' (Tucker, 1975). In large marine mammals, the primary forces are hydrodynamic drag, lift and buoyancy (Schmidt-Nielsen, 1997). Cost-of-transportation is a critical life-history feature that influences migration, foraging and social behaviour (Sumich, 1983; Connor et al., 1998), and natural selection should favor adaptations that reduce these costs (Vogel, 1981). A clear example of one such adaptation is the streamlined body form of marine mammals that results in decreased hydrodynamic drag compared to the ancestral body form (Williams, 1999). Other adaptations are apparent in mechanical structures such as fins to generate lift (Fish, 1996; Pabst, 1996), and behavioural flexibility to reduce energy outlays (Fedak and Thompson, 1993). Behavioural options that have been investigated include optimal swimming speed (Thompson et al., 1993) and swimming gait (Williams et al., 2000; Sato et al., 2003).

Hydrodynamic drag and basal metabolic rate are key determinants of optimal swimming speed to minimize cost-of-transportation (Fish and Hui, 1991; Williams et al., 1993). Low drag has obvious benefits for migrating animals, which may travel large distances without access to food (Sumich, 1983), and also for diving mammals, such as the sperm whale, which must travel between an oxygen source at the surface and food supplies at depth. A theoretical drag coefficient, based on a series of flat plates in a turbulent regime, was calculated as 0.0026 for the fin whale *Balaenoptera physalus* (Bose and Lien, 1989). Based on thrusting efficiency, Fish (1998) calculated the drag coefficient of fast-swimming killer whales *Orcinus orca* to be 0.0029. A drag coefficient of 0.0056 was calculated from glides for the Steller sea lion *Eumetopais jubatus* with Reynold's number of ~5×10^6 (Stelle et al., 2000).

Buoyancy forces, which can be stronger than drag forces, arise from gases carried by a diving animal and differences in density between non-gaseous animal tissues and the surrounding medium (Lovvorn and Jones, 1991; Beck et al., 2000). While buoyancy forces may have only a minor influence on horizontally transiting or migrating animals (Ogilvy and DuBois, 1982; Stelle et al., 2000), they add (or subtract) directly, to drag forces during vertical diving (Skrovan et al., 1999). While drag forces always oppose the direction of movement and increase with speed, buoyancy acts vertically and is not affected by speed. Buoyancy due to air carried by a diving animal is strongly affected by depth, with rapid changes in buoyancy near the surface as hydrostatic pressure reduces air volume. Buoyancy from tissue density is not much affected by pressure as both seawater and animal tissue have low compressibility (Skrovan et al., 1999). With the exception of polar waters, seawater temperature decreases (and density increases) with depth, which provides positive buoyancy to a diving animal as it moves into colder, deeper water (Clarke, 1970). Such temperature gradients may reduce external body temperatures during long dives in cold, deep water, particularly if blood flow to extremities is restricted (Schmidt-Nielsen, 1997). Tissue buoyancy also varies seasonally, as the amount of relatively light lipids carried by marine mammals changes between periods of feeding and fasting (Webb et al., 1998; Beck et al., 2000; Biuw et al., 2003).

Marine mammals employ diverse swimming styles referred to as ‘gaits’ (i.e. steady fluking, gliding, stroke-and-glide, porpoising) that appear to result in lower transportation costs when used in the appropriate conditions (Williams et al., 2000). Differences in buoyancy forces, both within dives and across animals, particularly influence use of glides during ascent and descent. Diving bottlenose dolphins glide more during descent after air volumes have collapsed due to hydrostatic pressure (Skrovan et al., 1999). Prolonged glides were made during descent by leaner Weddell seals *Leptonychotes weddellii*, while fatter seals employed stroke-and-glide swimming (Sato et al., 2003). Gliding during descent appears to reduce oxygen consumption, resulting in longer dives and more efficient foraging (Williams et al., 2000). Broadly speaking, species with negative buoyancy appear to glide more during descent (e.g. phocid seals, balaenopteridae; Williams et al., 2000), while positively buoyant species glide more during ascent (e.g. balaenids; Nowacek et al., 2001). The vertical velocity of elephant seals *Mirounga leonina*, whose buoyancy was altered experimentally, changed during descent, but ascent velocity appeared to be unaffected (Webb et al., 1998). Similarly, leaner grey seals *Halichoerus grypus* in the post-moult period had faster descent velocities, but also, seemingly paradoxically, faster ascent velocities (Beck et al., 2000). These different influences of buoyancy on descent and ascent velocities may reflect the fact that these animals glide during descent, but actively swim during ascent (Webb et al., 1998; Williams et al., 2000).

Sperm whales are accomplished divers, making dives greater than 1000 m depth and 1 h in duration (Watkins et al., 2002). Their ability to accomplish these dives successfully depends critically on the drag and buoyancy forces acting on them, and the speed and style of swimming employed to overcome these forces and successfully capture prey. There has been interest in the buoyancy of sperm whales at depth (see Whitehead, 2003), based upon the premise that sperm whales would benefit from obtaining neutral buoyancy at depth (Clarke 1970, 1978c). Clarke (1978c) analyzed factors affecting the relative density of a diving sperm whale and the seawater medium, and determined that if sperm whale tissue (without air) is neutrally buoyant at the surface, a whale would have a positive buoyancy of 100–650 N over much of its dive. To achieve neutral buoyancy, Clarke (1970, 1978c) proposed that sperm whales might increase tissue density by cooling oils in their massive spermaceti organ. Clarke (1970) further proposed that sperm whales might heat their oils actively during ascent to gain positive buoyancy. While this idea has been debated (Ridgway, 1971; Norris and Harvey, 1972; Cranford, 1999; Madsen et al., 2002; Whitehead, 2003), no data have been published to date reporting measurements of buoyancy or swimming patterns from diving sperm whales.

Our goal here is to describe the swimming behaviour of sperm whales, and to relate their behaviour to the drag and buoyancy forces acting on them. We detail the movements of diving sperm whales using a 500 g solid-state archival tag containing a depth sensor, an audio-band acoustic recorder, and 3-axis accelerometers and magnetometers. When sampled at high rates this sensor suite can be used to observe fine-scale details of the tagged whale’s behaviour, including its 3-D orientation, fluke strokes and vertical velocity (Johnson and Tyack, 2003). We analyze data from this instrument to describe the swimming gaits employed by sperm whales during deep dives and shallow surface dives. By fitting measured acceleration during glides to a model of drag and buoyancy forces, we obtain the first field estimates of drag and both air- and tissue-induced buoyancy forces that act on diving sperm whales.

Materials and methods

Field site and study animals

Field studies were conducted in the Ligurian Sea, in the Mediterranean Sea, from the R/V *Alliance* in 2000, 2001 and 2002. Studies in the Gulf of Mexico were undertaken from the R/V *Gordon Gunter* in 2000 and 2001, and from the R/V *Gyre* in 2002.

Tag design and attachment

We recorded the diving and swimming behaviour of sperm whales *Physeter macrocephalus* L. using a high-resolution digital recording tag ‘Dtag’ deployed on sperm whales using suction cups. The Dtag sensors include a hydrophone, a depth sensor, a temperature sensor, and 3-axis accelerometers and magnetometers (Johnson and Tyack, 2003).

Sperm whales were located at sea either by visual observers

on the flying bridge or acoustically using a towed hydrophone array. Once sperm whales had been located, visual and acoustic teams made initial observations from the R/V before a small rigid-hull inflatable boat was launched to attach tags to the sperm whales. Diving whales were tracked from the tag-boat using a custom-built directional hydrophone, and were approached upon surfacing. We approached whales at slow speeds, typically from directly behind, with the tag mounted on the end of a cantilevered 12 m-carbon pole (Moore et al., 2001). We sought to place the tag high on the animal, and most placements were just forward of the dorsal hump. Tag attachments were recorded using digital video and the response of the animal was carefully assessed.

Once the tag was applied to the animal, the team on the tag boat inspected the position of the tag on the animal, measured the whale's heading, and attempted to take identification photographs. The tagged whale was identified and followed *via* a VHF signal from the tag along with visual and acoustic tracking (Lerczak and Hobbs, 1998; Zimmer et al., 2003). Once the tag detached from the animal, it was retrieved from the sea surface by tracking the VHF signal. CTD casts were often made from the research vessel near the location where tags were recovered. Suction cups were inspected for the presence of sloughed skin, which was preserved in DMSO and subsequently genetically analyzed to determine the sex of the tagged animal (Berube and Palsbøll, 1996). The magnetometers on the tag were calibrated immediately on retrieval to account for the remanent magnetic field held by steel and nickel components in the tag. A least-squares fitting method was used to reduce temperature- and pressure-related offsets in the 3-axis accelerometer and magnetometer signals (Johnson and Tyack, 2003).

Length estimation/allometry

Estimation of drag and buoyancy parameters described below requires values for each whale's length, mass and surface area. To obtain these values for tagged whales, observers on the tagging boat made calibrated video recordings at measured ranges from tagged whales resting at the surface ('logging'). We positioned the small boat directly broadside of the logging whale at >100 m range and took frame images of the whale using a calibrated Canon GL1 digital video recorder at a fixed zoom setting (full zoom). The range to the logging whale was measured using a Bushnell Yardage Pro 1000 range finder (accuracy of ±1 m) and recorded by voice on the audio channel of the video recorder. To ensure that the logging whale was oriented broadside to the camera, we took multiple measurements as we moved from slightly behind to slightly ahead of broadside of the logging animal. In several cases we were able to confirm the broadside orientation of the whale by inspection of the tail flukes when the whale dived.

Digital images were transferred from the camera to computer. The number of pixels from the blow-hole to the dorsal fin was measured, and this measurement was converted to centimeters based upon the range to the whale and the camera calibration factor. The camera was calibrated at the full zoom setting using a measuring tape at measured ranges from 16 to 180 m to determine the conversion factor of pixels to degrees. In addition, we measured the length of several known-length targets at sea, with an error of less than 1.0%.

Having obtained the distance from the blow-hole to the dorsal hump, this distance was converted to animal length, mass and surface area based upon published analyses of sperm whale allometry. Total animal length was estimated using Gordon's equation (Gordon, 1990) with a small correction of half of the dorsal fin width (Fujino, 1956) as Gordon's equation was based upon the rear end of the dorsal while we measured the tip of the dorsal. Gordon's equation for length ($\text{length}=0.3875+1.679\times db-0.015\times db^2$), where db is the distance from the dorsal to blowhole) was based upon 188 male and female sperm whales and was a good fit for animals of size ranging from 2 to 17 m in length (see fig. 3 in Gordon, 1990). This technique was used to estimate the length of all of the whales except sw250, for which we estimated length based upon the position of tag-placement and the length of the tagging pole from a digital video recording.

Animal length was subsequently converted to an estimate of animal mass in metric tons (10^3 kg) using Lockyer's equation ($1.25\times0.0196\times\text{length}^{2.74}$; Lockyer, 1976), where the 1.25 multiplier accounts for blood loss for animals weighed in parts (Rice, 1989). Surface area of the tagged whales was estimated as ($0.37\times\text{length}^2$), based upon Clarke's measurement (Clarke, 1978a) of the surface area of four whales ranging from 9.4 m to 15.2 m in length. The fineness ratio (length/maximum diameter) of sperm whales appears to be largely unaffected by animal length, and ranges from 5.55 for a 8 m juvenile to 5.48 in a 14 m adult male (Clarke, 1978a; Lockyer, 1991). We used a value of 5.50 to calculate the theoretical drag of a spindle of the same fineness ratio as the sperm whale.

Tag data analysis

Data downloaded from the Dtag were analyzed to obtain high-resolution depth and 3-dimensional orientation values. Raw sensor data were initially filtered and down-sampled by eight times (four times for sw250) to obtain a common effective sampling rate of 5.88 Hz across all tag deployments. Pressure readings on the depth sensor were converted to meters using calibrated values, and magnitude readings from the 3-axis accelerometers and magnetometers were converted to pitch, roll and heading of the tag in the earth frame, following the technique described in detail in Johnson and Tyack (2003). We derived the 3-dimensional orientation of the whale in the earth frame by correcting for the orientation of the tag on the whale. This correction was estimated based upon visual inspection of the position of the tag on the whale, and then refined using measured values of the heading of the whale at the surface. The criteria for an accurate tag-frame to whale-frame conversion were: (1) whale pitch and roll should equal zero when the whale was resting at the surface; (2) whale headings measured by the tag should match those measured visually; (3) the rapid change in pitch upon diving should not correspond with a change in roll; and (4) the tag-frame to

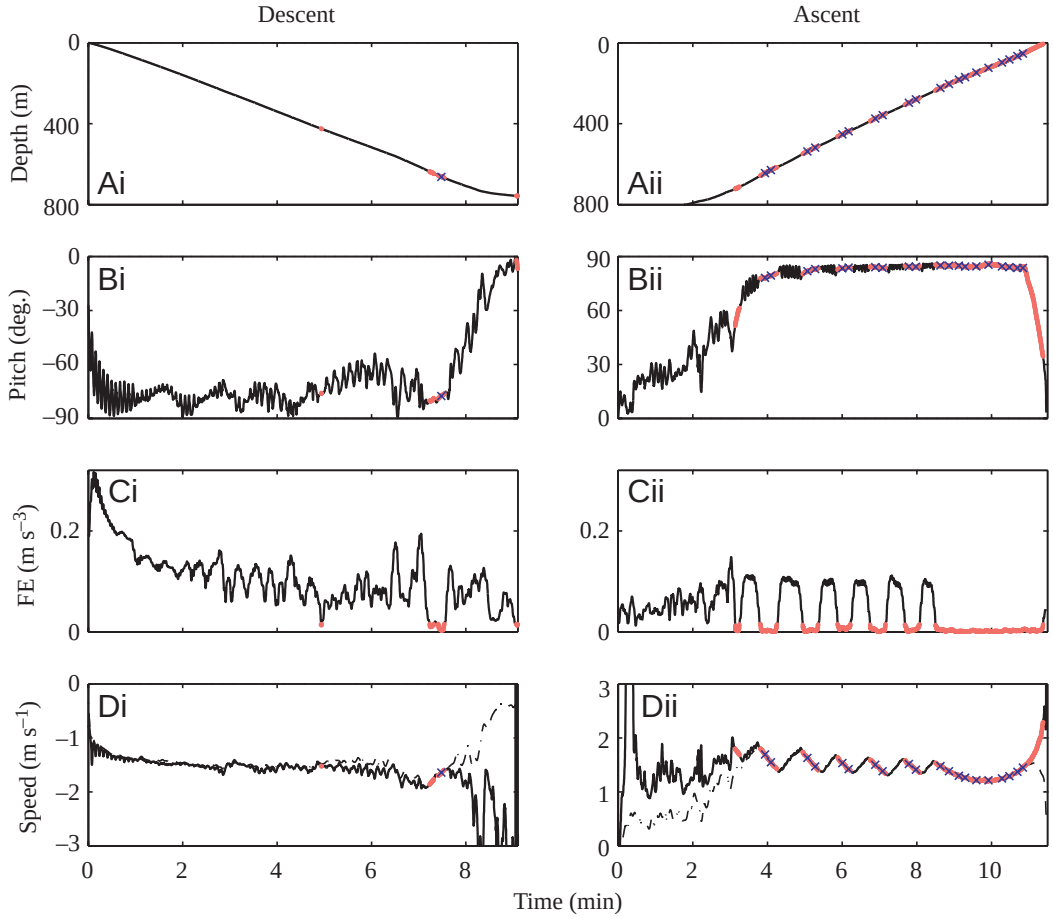

Fig. 1. Examples of measurements of data from Dtag during the descent and ascent of the fourth dive recorded from animal sw275b. In all panels, gliding periods are colored light red and thrusting periods black. Each blue cross marks the position at which depth, pitch, speed and acceleration values were measured from descent (Ai–Di) and ascent (Aii–Dii) glides. The beginning of a descent was the time the whale left the surface, while the end was the time when whale pitch first exceeded 0° (i.e. when was no longer oriented downward). Conversely, an ascent was defined to start at the last point in time when an animal's pitch was downward (<0°) and ended when the whale reached the surface. (A) Depth *versus* time; (B) pitch of the whale (note the oscillations in pitch caused by fluking by the whale); (C) fluking energy (FE; see text for further details); (D) speed through the water, calculated as vertical velocity (broken line) divided by sin(pitch). Note the oscillations in speed corresponding to the acceleration of the whale during glide and thrusting intervals.

whale-frame conversion should match the visually inspected orientation of the tag on the whale.

Tag records were divided into five exclusive intervals: surface time, descent phase of dive, bottom period of dives, ascent portion of dives and shallow dives. The beginning of a descent was the time the whale left the surface, while the end was the time when whale pitch first exceeded 0° (i.e. when it was no longer oriented downward). Conversely, an ascent was defined to start at the last point in time when an animal's pitch was downward (<0°) and ended when the whale reached the surface. Dives were considered to be 'shallow' if the whale did not exceed 350 m depth. For ascent and descents of deep dives, we calculated the mean pitch and vertical velocity. These values were averaged for each whale, and the mean values were averaged across whales.

We measured the percentage of time each whale was actively thrusting with its flukes ('fluking') during descent and ascent periods. Fluking can be detected clearly on the tag record as oscillations in the pitch record or in the raw accelerometer signals themselves with a period ranging from 6–8 s (Nowacek et al., 2001; Johnson and Tyack, 2003). This method of observing active fluking can be confirmed by listening to low frequency flow noise over the tag, which also oscillates with fluking. We used acceleration values in the whale's *Z*-axis (dorsal–ventral), based on the correction of tag-placement described above (Fig. 1B) to quantify when the whale was fluking *versus* gliding. First we calculated the rate of change in *Z*-axis accelerations or 'jerk' by taking the difference in successive accelerometer values. To reduce noise from non-fluking perturbations to pitch, we band-pass filtered jerk to periods of 4–10 s. Filtered jerk was squared, averaged and square-rooted over the period of a typical fluke stroke (5.4 s or 32 samples) to obtain root mean-square jerk as a metric of fluking-energy (Fig. 1C). Most ascents had a long terminal glide, and a threshold of 3× the fluking energy during these glides was used as a threshold to identify gliding periods

in the dive records. The accuracy of this threshold was checked visually. Individual whales oscillated their flukes at a consistent frequency, so gliding time is inversely proportional to mean overall thrusting rate, as defined by Sato et al. (2003).

Drag and buoyancy forces during glides

In order to describe the forces acting on diving sperm whales, we developed a model of drag and buoyancy based upon the anatomy of sperm whales. We explored how well this model fit accelerations during glide periods using a modified version of the method described by Bilo and Nachtigall (1980) including equations from Skrovan et al. (1999) and Sato et al. (2002). The assumption in the method described by Bilo and Nachtigall (1980) is that animal acceleration during a glide is solely a function of drag forces; any buoyancy effects are ignored. For a whale ascending at a steep pitch, however, vertical buoyancy forces contribute to the forces affecting caudal–rostral acceleration during a glide as a function of sin(pitch) (Fig. 2; Sato et al., 2002). Buoyancy is equal to the mass of the fluid displaced by a body minus the mass of the body, and is considered positive when the mass of the displaced fluid exceeds that of the body. Dividing the body into air and non-air tissue portions, this can be expressed as:

$$F_b = \boldsymbol{g} \cdot \rho_w(V_{air} + V_{tissue}) - \boldsymbol{g}(\rho_{air} \cdot V_{air} + \rho_{tissue} \cdot V_{tissue}) , \quad (1)$$

where F_b is the total force of buoyancy, ρ_w is density of the displaced seawater, V_{air} is the volume of air carried by the whale, V_{tissue} is the volume of whale tissue, $\boldsymbol{g}$ is the gravitational constant, and ρ_{air} and ρ_{tissue} are the mean densities of air and whale tissue, respectively. Equation 1 can be rewritten as:

$$F_b = \boldsymbol{g} \cdot V_{air}(\rho_w - \rho_{air}) + \boldsymbol{g} \cdot V_{tissue}(\rho_w - \rho_{tissue}) . \quad (2)$$

Adding the drag force and setting: $F_{drag}+F_b=ma$, where m is the mass of the body, a full expression of the forces affecting acceleration during a glide is:

$$a = \underbrace{\frac{C_d \cdot 0.5 \cdot \rho_w \cdot A \cdot v^2}{m_{tissue} \cdot m_e}}_{\text{Term 1}} + \underbrace{\frac{V_{air} \cdot \sin(p) \cdot \boldsymbol{g} \cdot (\rho_w - \rho_{air})}{m_{tissue} \cdot m_e}}_{\text{Term 2}} + \underbrace{\frac{\sin(p) \cdot \boldsymbol{g} \cdot V_{tissue} \cdot (\rho_w - \rho_{tissue})}{m_{tissue} \cdot m_e}}_{\text{Term 3}} , \quad (3)$$

where a is the acceleration observed during the glide, C_d is the drag coefficient, A is the surface area of the whale, v is speed through the water, m_{tissue} is the mass of the whale, m_e is a multiplier for entrained water attached to the surface of the whale (total $m=m_{tissue} \cdot m_e$), and p is the pitch of the whale. Term 1 describes the effect of drag forces on animal acceleration during glides, and is a function of v^2 for any given whale. Because the accelerations were measured from glides naturally produced by steeply ascending whales, we assume that use of control surfaces to generate lift is negligible (Sato et al., 2002). Animal roll, pitch and heading were stable during glides, and whales should maximize their movement efficiency during ascents from a long and deep dive. Terms 2 and 3 are the air and tissue buoyancy forces, respectively, and are each weighted by the sine of the animal's pitch during the glide (Fig. 2).

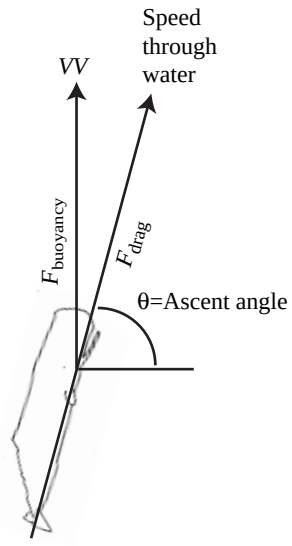

Fig. 2. Geometry of movement and forces acting on an ascending sperm whale. Here the whale is oriented at an ascent pitch θ of 75°. *VV*, or vertical velocity, of the whale can be accurately measured as the change of depth. Speed through the water is then equal to the absolute value of *VV*/sinθ. Drag forces on the whale, F_{drag}, act directly in line against the movement of the whale through the water. Buoyancy forces, $F_{buoyancy}$, act vertically so the effect of buoyancy forces on speed through water are weighted by sinθ when added to drag forces.

The influence of glide depth

The depth of a glide affects many of the terms in Equation 3. Seawater density ρ_w is the only depth influence on term 1 and can be calculated for any depth using CTD profiles near tag locations to obtain salinity and temperature (Fofonoff and Millard, 1983; Morgan, 1994). Air volume at depth is equal to air volume at the surface (diving lung volume) divided by (1+0.1d) according to Boyle's Law, where d is depth in meters. Conversely, the density of air ρ_{air} increases with (1+0.1d). The term (ρ_w–ρ_{air}) changes only slightly with respect to depth as water is highly incompressible and ρ_{air} is small compared to ρ_w. In the Ligurian Sea, (ρ_w–ρ_{air}) is (1027.3–4.8) or 1022.5 kg m^{-3} at the shallowest analyzed glide depth of 38 m and (1030.5–76.7) or 953.8 kg m^{-3} at the deepest glide depth of 757 m, a decrease of only 6.5%.

With full depth effects, term 2 of Equation 3 can be written as:

$$\text{Term 2} = \ldots \frac{V_{air}(0)}{m_w} \cdot \frac{\sin(p) \cdot \boldsymbol{g} \cdot [\rho_w(d) - \rho_{air} \cdot (1+0.1d)]}{(1+0.1d) \cdot m_e} \ldots , \quad (4)$$

where $V_{air}(0)$ is the air volume carried by the whale at the surface (d=0) and ρ_{air} is defined as the density of air at the surface.

The density of animal tissue in term 3 is a function of both pressure and temperature. Most animal tissues have the same compressibility as seawater (Skrovan et al., 1999; Beck et al., 2000). While certain tissues such as blubber are somewhat more compressible than water, others such as bone are less

compressible (Clarke, 1978c). Therefore, we can neglect the pressure influence of animal depth on tissue buoyancy as compression equally increases the densities of tissue and displaced seawater.

While we can assume that the whale is at ambient pressure at depth, we cannot assume that it is at ambient temperature, and the influence of seawater temperature changes with depth may be substantial if whale temperature is constant (Clarke, 1970). The colder and denser water that the whale displaces at depth creates a positive buoyancy force relative to when the whale is at the surface. The force is equal to the temperature-induced density change of the displaced seawater. One way to visualize this is to imagine that the whale is equivalent to an insulated bag of seawater, which can be maintained at a different temperature from the surrounding seawater. The difference in density of the warm bag of water from that of the displaced fluid is defined as $\Delta\rho_w(T)$, which can be determined from CTD data. For example, in the Mediterranean Sea, seawater is roughly 20° near the surface and decreases to 13° at 1000 m. At 1000 m depth, the densities of seawater at 13°C and 20°C are 1034 kg m^{-3} and 1032 kg m^{-3}, respectively. Thus, the value for $\Delta\rho_w(T)$ is 2 kg m^{-3}, which is the effect of the temperature difference at 1000 m depth at this location. Note that the $\Delta\rho_w(T)$ term is quite small compared to the actual density.

If the density of tissue is assumed to remain constant with respect to temperature, but varies equally with the surrounding seawater with respect to pressure, the depth-dependence of term 3 can be written as:

$$\text{Term 3} = \left(\frac{\rho_w + \Delta\rho_w(T)}{\rho_{tissue}} - 1 \right) \cdot \frac{\sin(p) \cdot \boldsymbol{g}}{m_e} , \qquad (5)$$

in which $\Delta\rho_w(T)$ is calculated as explained above for the temperature of the seawater at each glide depth, *versus* a reference temperature near the surface (40 m depth). Thus, the terms ρ_w and ρ_{tissue} are referenced to 40 m depth as well. Note that V_{tissue}/m_{tissue} is equal to $1/\rho_{tissue}$, which simplifies term 3.

Rewriting Equation 3 in matrix form with full depth-dependencies obtains the following model of glide forces:

$$\mathbf{A} = \left[\mathbf{D}\{v^2\}\, \mathbf{B_{air}} \left\{ \frac{1}{(1+0.1d)} \right\} \mathbf{B_{tissue}} \right] \begin{bmatrix} C_d \\ \dfrac{V_{air}(0)}{m_{tissue}} \\ \dfrac{\rho_w}{\rho_{tissue}} - 1 \end{bmatrix} + \frac{\Delta\boldsymbol{\rho}_\omega(T)}{\rho_{tissue}} \cdot \frac{\sin(\mathbf{P}) \cdot \boldsymbol{g}}{m_e} , \qquad (6)$$

where **A** is the vector of measured accelerations during an ascent and **P** is the vector of animal pitches during each glide. **D** is the vector of known values of each glide from the first term in Equation 3 except the drag coefficient C_d, and is a function of the square of speed. $\mathbf{B_{air}}$ is the vector of known values from the second term in Equation 3 excluding $V_{air}(0)/m_{tissue}$, and is a function of the pressure effect on air volume. $\mathbf{B_{tissue}}$ is $\sin(\mathbf{P})\cdot\boldsymbol{g}/m_e$, and is not influenced directly by depth or speed. The $\Delta\rho_w(T)/\rho_{tissue}$ term can be estimated closely as $\Delta\rho_w(T)/\rho_w$ because the value of $\Delta\boldsymbol{\rho}_w(T)$ is small compared to ρ_w or ρ_{tissue}.

Model fit and estimation of drag and buoyancy parameters

Our goals are to use experimental measurements of animal depth D, pitch p, speed v, acceleration a, mass m and area A, to estimate values for the unknown coefficients C_d, $V_{air}(0)/m_w$ and $\rho_w/\rho_{tissue}-1$ and to determine how accurately the model fits the observed data.

We only conducted this detailed analysis for sperm whales from which we had recorded at least two 'steep' ascents, because this analysis requires multiple glides by whales at high pitch across a range of depths and speeds. 'Steep' ascents are defined as ascents in which the whale maintained a pitch of 60° or higher up to a depth of 50 m and maintained a fairly consistent vertical velocity (i.e. no pauses during ascent). In ascents classified as 'non-steep', whales reduced their pitch at various times throughout the ascent, presumably to translate their position horizontally during ascent.

Animal speed through the water v, depth D and pitch p were taken as the mean value during each glide period measured (Fig. 1). We calculated speed through the water as: $\delta D/\sin p$, based on the assumption that lift forces are minimal and the whale moves in a caudal–rostral direction through the water (Fig. 2). The minimum pitch angle for which we attempted to calculate speed through the water was 50°, for which the correction is 30.5%. At the average pitch of 79.6°, the correction is only 1.7%. To increase the range of glide velocities, we divided most glides in half into two sub-glides except the long terminal ascent glide, which we divided into multiple sub-glides depending on its duration (Fig. 1). Acceleration during each sub-glide was measured directly using a linear regression of speed *versus* time. We found the change in speed *versus* time to be quite linear in the sperm whale glides, so it was not necessary to use inverse speed as suggested by Bilo and Nachtigall (1980). For each sub-glide we obtained a Reynold's number (Re) using the animal's length estimate and the mean speed during the sub-glide (Vogel, 1981). The value for m_e was set to 1.06 based on the measure for a prolate spheroid of fineness ratio 5.0 (Skrovan et al., 1999).

The linear coefficients C_d, $V_{air}(0)/m_{tissue}$ and $(\rho_w/\rho_{tissue}-1)$ were then estimated using linear least-squares fitting (Strang, 1991) for each whale. Linear least-squares estimation of the unknown terms in Equation 6 is equivalent to fitting the observed acceleration data to a 3-term regression model with no constant (Zar, 1984). The slopes of the three terms in the regression are the estimates for C_d and $V_{air}(0)/m_{tissue}$, and $\rho_w/\rho_{tissue}-1$. The statistics of the model fit were obtained by fitting all sub-glides from each whale to a 3-term linear regression model with no constant in Systat (Zar, 1984), using a P-value of 0.01. For each whale, all three coefficients were

Table 1. *Descriptive information for tag deployments with at least one complete dive*

Animal	Sex	Length (m)	Location	Month/year	Dive duration (h)	Number of entire dives	Number of steep (>60°) ascents
Sw250	m*	12.9	LS	09/2000	4.6	3	2
Sw265	m*	12.7	LS	09/2001	4.3	4	4
Sw275b	m*	12.2	LS	10/2001	6.9	8	8
Sw189b	M	–	LS	07/2002	0.7	1	0
Sw191b	m*	13.4	LS	07/2002	5.1	5	4
Sw200	F	9.2	GM	07/2001	8.4	8	0
Sw204	F	8.5	GM	07/2001	5.3	6	1
Sw208b	M	12.4	GM	07/2001	2.9	1	0
Sw209c	–	10.0	GM	07/2001	2.9	4	2
Sw235c	F	–	GM	08/2002	1.3	1	1
Sw237a	F	–	GM	08/2002	3.3	2	0
Sw238a	F	–	GM	08/2002	3.8	3	0
Sw238b	–	–	GM	08/2002	2.1	3	1
Sw239a	F	9.9	GM	08/2002	12.4	12	0
Sw239b	–	10.0	GM	08/2002	0.9	1	0
Sw240a	–	–	GM	08/2002	0.7	1	0
Sw240c	–	9.3	GM	08/2002	5.2	5	2
Sw248a	–	–	GM	09/2002	0.9	1	0
Sw249a	–	–	GM	09/2002	1.9	2	0
Sw253a	–	–	GM	09/2002	3.7	3	0
Sw254a	F	–	GM	09/2002	11.4	11	4
Sw254b	F	–	GM	09/2002	12.4	9	1
Sw254c	–	–	GM	09/2002	12.4	10	0

LS, Ligurian Sea; GM, Gulf of Mexico.

Sex was determined using genetic analysis of skin recovered with tag except for m*, which refers to sex-attribution based upon size or behavior.

first estimated using all ascent sub-glides from all dives. Because $V_{air}(0)$ can vary between dives, the C_d and $\rho_w/\rho_{tissue}-1$ coefficients were constrained by the overall estimates, and $V_{air}(0)/m_{tissue}$ was then estimated separately for each dive. An estimate was made of the drag coefficient C_d for each sub-glide by subtracting the effect of the buoyancy terms, and C_d was compared to the Reynold's number (Re) of each sub-glide.

The fit of the model (r^2) to the observed acceleration data was calculated for each whale and the model was used to predict acceleration during descent glides made by the same whale. A check against descent glides is important because drag and tissue-buoyancy may be inter-correlated when only ascent glides are used to build the model, and the range of speeds observed is limited. There is less concern for inter-correlation with air-buoyancy because glides were measured over a large depth range. The direction of the drag force is reversed during descent, so testing descent predictions provides a strong test of the overall accuracy of the model.

Results

We attached Dtags to a total of 40 sperm whales, seven of which were in the Ligurian Sea and the rest in the northern Gulf of Mexico (Table 1). We recorded at least one entire deep dive from 23 sperm whales, and two or more deep dives from 17 whales (Table 1). Typical reactions to approach and tagging were minor and of short duration, such as a brief startle response following by an arch-out dive.

Swimming gaits/gliding rates

In order to describe fluking patterns during descent, ascent and shallow dives for the same individual, we limited our analyses to the 23 whales from which we recorded at least one complete deep dive (Tables 1, 2). Descent was marked by a steep initial descent, with small oscillations in downward pitch, steady changes in roll and active clicking (Fig. 1; see also Zimmer et al., 2003). Whales fluked actively during descent and maintained a fairly constant speed through the water (Figs 1, 3). Ascents generally had an early phase of low-pitch ascent with steady fluking, followed by a later phase of steeper ascent with significant gliding and few changes in roll (Figs 1, 3).

Whales descended at a mean (± S.D.) vertical velocity of 1.15±0.14 m s^{-1} at a mean pitch of –53.3±6.3° (Table 2). Vertical velocity during ascent averaged 1.33±0.16 m s^{-1} at a mean pitch of 56.6±10.4°. Vertical velocity was generally quite constant during steady fluking, but oscillated during stroke-and-glide swimming (Figs 1, 3). The magnitude of the pitch angle did not differ between ascent and descent (paired t_{22}=1.84, P=0.08), but vertical velocity was higher during ascent than descent (paired t_{22}=5.20, P<0.001). Correcting ascent/descent velocity for animal pitch (Fig. 2) obtains a mean

Table 2. *Swimming and fluking behavior of deep-diving sperm whales*

	Descent				Ascent			
Animal	Velocity (m s^{-1})	Pitch (degrees)	Glide (%)	Primary gaits	Velocity (m s^{-1})	Pitch (degrees)	Glide (%)	Primary gaits
sw250	1.39±0.07	–55.3±4.3	2.6±2.3	3-f	1.65±0.08	58.8±3.6	38.3±5.3	3-sg
sw265	1.22±0.12	–59.9±2.6	0	4-f	1.33±0.03	78.4±3.9	47.2±6.5	3-sg
sw275b	1.23±0.14	–58.3±9.7	1.1±1.2	8-f	1.24±0.12	67.1±8.6	45.1±7.3	8-sg
sw189b	1.55	–56.2	6.0	1-f	1.51	58.2	27.7	1-sg
sw191b	1.21±0.08	–59.7±7.3	2.0±2.5	5-f	1.49±0.07	71.7±5.3	39.1±8.1	5-sg
sw200	0.94±0.22	–48.5±5.9	0.3±0.6	9-f	1.10±0.15	44.4±7.6	58.3±15.6	4-pg, 4-sg
sw204	1.26±0.10	–59.7±1.6	1.9±1.0	6-f	1.29±0.16	49.6±10.5	23.6±16.8	3-f, 3-sg
sw208b	1.03	–57.8	3.2	1-f	1.16	47.7	31.7	1-sg
sw209c	1.13±0.13	–46.4±2.3	1.3±1.6	4-f	1.26±0.31	49.3±11.9	40.1±12.6	1-f, 3-sg
sw235c	1.26±0.07	–58.6±0.7	0.6±0.8	2-f	1.31	69.3	18.4	1-sg
sw237a	1.10±0.13	–59.7±2.7	2.1±0.5	2-f	1.46±0.11	55.0±1.1	52.9±11.7	2-sg
sw238a	1.09±0.10	–59.4±9.6	10.1±10.3	3-f, 1-sg	1.28±0.05	61.2±2.7	34.9±12.5	3-sg
sw238b	1.20±0.08	–53.0±1.3	7.4±6.8	3-f	1.42±0.27	64.4±2.9	41.2±5.2	3-sg
sw239a	1.17±0.17	–57.5±5.7	1.7±2.8	13-f	1.14±0.10	43.0±7.5	46.6±14.3	12-sg
sw239b	1.03	–58.0	1.1	1-f	1.15	63.3	27.3	1-sg
sw240a	1.13	–58.2	10.6	1-sg	1.71	61.2	22.7	1-sg
sw240c	0.89±0.20	–52.9±4.2	9.3±8.9	1-f, 4-sg	1.40±0.15	65.8±9.7	28.7±11.5	5-sg
sw248a	1.15	–40.3	23.1	1-sg	1.40	39.7	2.6	1-f
sw249a	1.17±0.16	–48.3±1.2	16.6±2.5	2-f	1.20±0.15	62.5±3.5	9.4±7.6	1-f, 1-sg
sw253a	1.06±0.13	–46.0±10.1	0.0	4-f	1.28±0.19	48.9±8.2	67.7±19.3	2-sg, 1-pg
sw254a	0.98±0.16	–42.2±10.4	2.1±3.2	12-f	1.36±0.21	50.5±11.2	57.6±14.6	10-sg, 1-pg
sw254b	1.23±0.12	–49.3±6.4	16.9±8.2	3-f, 7-sg	1.24±0.23	49.8±8.9	15.9±6.3	4-f, 5-sg
sw254c	1.09±0.21	–43.7±10.1	2.0±2.5	11-f	1.23±0.22	42.3±7.8	51.1±17.0	9-sg, 1-pg
Overall mean	1.15±0.14	–53.3±6.3	5.3±6.3		1.33±0.16	56.6±10.4	36.0±16.4	

Values are means ± S.D., when more than one dive was recorded.

Gaits, the number of descents or ascents in which the primary swimming gait was either: steady fluking (f), stroke and glide (sg), or prolonged glide (pg) of over 300 m depth. For example '3-f, 1-sg' indicates three separate dive descents (or ascents) with steady fluking, and one with stroke-and-glide swimming.

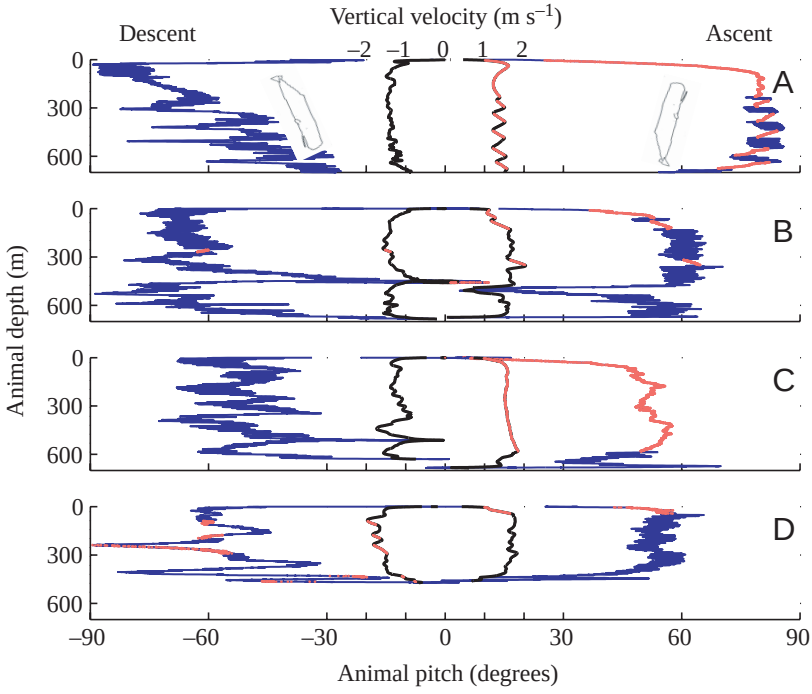

Fig. 3. Pitch and vertical velocity of sperm whales during descent (left side of each panel), and ascent (right side of each panel). Periods of gliding are marked in light red on the pitch and velocity traces. (A) The most commonly observed pattern, with steady fluking during descent and stroke-and-glide swimming during the ascent. Note that the ascent in A is considered a 'steep' ascent as pitch is >60° throughout and there are no pauses during the ascent. This same ascent is shown in more detail in Fig. 1. (B) Another example of predominantly active fluking during descent with stroke and glide during ascent. This ascent is considered 'non-steep' as pitch is often less than 60°. The dive in (C) reveals steady fluking during the descent, but prolonged gliding of almost 600 m during the ascent. In (D), the whale use a stroke-and-glide swimming gait during descent and primarily steady fluking during ascent.

descent speed through water of 1.45±0.19 m s^{-1}, which was significantly lower than the pitch-corrected mean ascent speed of 1.63±0.22 m s^{-1} (paired t_{22}=4.04, P<0.001).

All sperm whales exhibited strong fluking at the beginning of descent and gliding during the terminal phase of the ascent for all dives (Fig. 3), probably reflecting the buoyancy effect of air carried from the surface. Overall, mean gliding time was much lower during descent (5.3±6.3%) than ascent (36.0±16.4%) phases (paired t_{22}=6.8, P<0.001). The most common swimming gait observed was steady fluking during descent, and stroke-and-glide during ascent (Figs 1, 3A,B). This pattern was observed during all dives for 12 individuals and during at least a subset of dives for another 10 whales (Table 2).

Inter-individual variability of percentage time gliding (with coefficients of variation of 119% for descent and 44% for ascent) was greater than for all other measures of dive behaviour. Twenty whales glided more during ascent than descent, while three individuals glided somewhat more during descent than ascent (Table 2). Across these 23 whales, there was a significant negative relationship between the percentages of time gliding on ascent *versus* descent (Spearman rank r=–0.59, P<0.0001), consistent with the expectation that tissue buoyancy should affect gliding behaviour inversely on ascent *versus* descent.

Inter-individual variability of swimming gaits corresponded to that in percentage time gliding. Four sperm whales showed evidence of stronger than average positive buoyancy by fluking steadily during descent and making at least one prolonged glide over 350 m during an ascent (e.g. Fig. 3C). Conversely, some other individuals showed evidence of less positive buoyancy. As noted above, three whales glided more during descent than ascent. Also, five sperm whales did predominantly stroke-and-glide swimming during at least one descent, and two of these also fluked steadily during at least one ascent (Table 2).

A total of 59 shallow dives were recorded from 13 of the 23 whales. These dives had a mean duration of 11.96 min (S.D.=6.5; min., 2.82; max., 31.47) and a mean maximum depth of 16.3 m (S.D.=12.0; min., 3.6; max., 64.23). The predominant swimming gait during 30 of these dives was stroke-and-glide, while steady fluking was observed in 26 dives. During three shallow dives, whale sw254a (which made one prolonged glide from a deep dive; Table 2) maintained a steady depth less than 20 m with its head oriented toward the surface for 14.1, 11.3 and 11.1 min. During these shallow dives, there was no change in depth, there was no flow noise audible acoustically, and no fluking was apparent in the accelerometer records until the whale moved to the surface. The sound of bubbles from released air was audible during these dives, with a near simultaneous slowing of ascent by the whale. We conclude that the animal was resting during these intervals and modulated its air content to achieve neutral buoyancy.

Data usable for drag and buoyancy model

We were able to obtain video-photogrammetry measurements from eleven whales, of which eight had at least two complete dives (Table 1). Measured lengths ranged from 8.5–13.4 m. All tagged whales in the Ligurian sea were confirmed or probably male and exceeded 12 m in length. Whales in the Gulf of Mexico were generally less than 10 m in length except for sw208b, which was 12.4 m and confirmed male. Three of the smaller Gulf whales were confirmed to be female, while the others were either adult females or adolescent whales of unknown sex.

Five of the eight measured whales (sw250, sw265, sw275b, sw191b and sw209c) had at least two steep ascents and thereby met the criteria for detailed analysis of drag and buoyancy parameters (Table 1). All five whales utilized the most commonly observed swimming gait of steady fluking during descent (gliding 0.6–6.4%) and stroke-and-glide swimming during ascent (gliding 43.0–52.0%; Table 2). These five whales were either isolated animals or in a widely spaced social aggregation associated with males (Lettevall et al., 2002).

From these five whales, we recorded a total of 20 steep ascents, and extracted a total of 382 sub-glides for analysis. The sub-glides had a mean (± S.D.) duration of 10.2±4.5 s and pitch of +79.6±7.0° covering a depth range of 38–757 m. Speed through the water during glides ranged from 1.1 to 2.2 m s^{-1}, with an overall mean of 1.5±0.2 m s^{-1}. Accelerations ranged from –0.023 m s^{-2} to +0.012 m $s^{-2,}$ and were strongly affected by both animal depth and speed through the water (Fig. 4).

Evaluation of the drag and buoyancy models

Using Equation 6 above, we fit the observed accelerations to the model of glide forces, obtaining estimates for drag coefficient C_d, air carried to depth [$V_{air}(0)/m_{tissue}$] and animal density ρ_{tissue}. The model fit measured accelerations with an r^2 of 99.1–99.8% for each whale, average 99.6%. All three terms

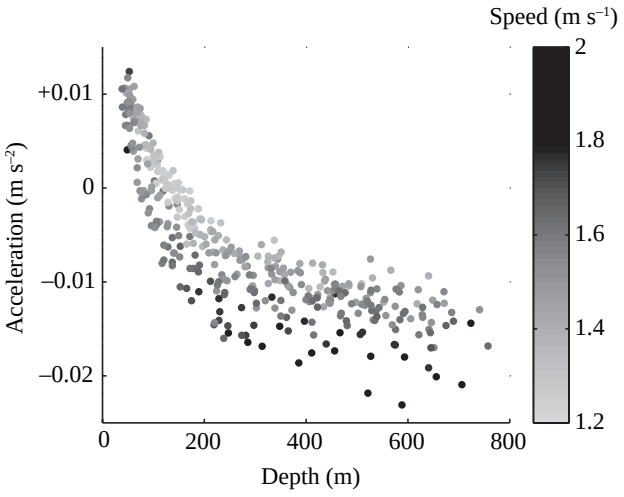

Fig. 4. Acceleration during glides as a function of glide depth and speed (gray-scaling). Note the strong change in acceleration from negative to positive values at depths less than 200 m, due to increased buoyancy from expanding air within the sperm whale. The effect of speed as predicted by the drag equation is apparent, since accelerations within any depth range were lower when the glide speeds were higher.

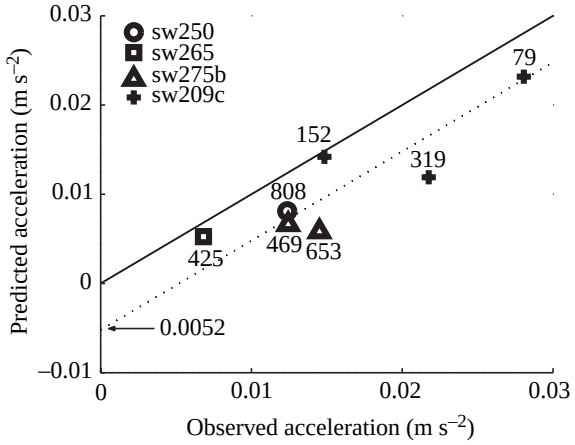

Fig. 5. Observed *versus* predicted acceleration during seven descent glides. Predicted descent glide accelerations are calculated using coefficients estimated from ascent glides for each whale. The number close to each data point is the mean depth of the descent glide. Predicted and observed values are positively correlated with a slope of 0.95 (P<0.01). The average offset of predictions from observed values is calculated by fitting a line with slope of 1.0 (dotted line) to the data yielding a y-intercept of –0.0052 m s^{-2}. This offset could be explained by an average tissue-density decrease of 0.064% between ascents and descents due to tissue warming while the whale is at the surface.

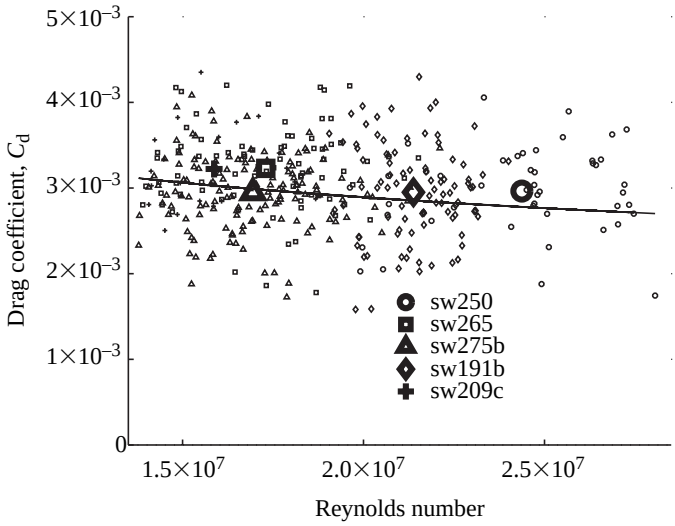

Fig. 6. Estimate of drag coefficient C_d *versus* Reynold's number for the sub-glides analyzed from five sperm whales. Individual sub-glides are shown as small symbols, and the mean for each animal is the large symbol. The black line is the theoretically derived drag coefficient for a completely turbulent spindle of fineness ratio 5.50 (see Stelle et al., 2000). Note that the mean drag coefficient for each animal is quite close to the theoretical level for a turbulent spindle, and that there is little variation across animals in the drag estimate.

were statistically significant at P<0.01 for all whales. Error residuals *versus* depth were quite flat ($F_{1,380}$=0.02, P=0.96), suggesting that the model adequately accounted for depth-specific effects acting on acceleration.

Because gliding during descent was quite rare, we identified a total of only seven descent glides by four of the five animals that were both of sufficient duration and steep enough pitch for acceleration to be reliably measured. We compared these measured descent accelerations to predicted values derived from ascents based on Equation 6. The slope of predicted *versus* observed glide accelerations was 0.80 (t_5=4.04, P<0.01), and not significantly different than 1.0, which is the expected value for a model fit (Fig. 5). The mean difference between observed descent-glide accelerations and predicted values was –0.0052 m s^{-2}.

Thus, the model of glide forces had a statistically strong fit to ascent glide accelerations (r^2 = 99.1–99.8%), and the model based upon ascent data correlated with descent glide accelerations with a small constant offset. Based on the mass of the different whales, this offset is consistent with a decrease in whale density of 0.064% during the surfacing interval between an ascent and the subsequent descent.

Drag and buoyancy parameters

Treating individual whales as the unit of analysis, the mean estimate (± S.D.) for the drag coefficient C_d was 0.00306±0.00015 (Table 3). The estimate of the drag coefficient was close to the predicted value for a completely turbulent spindle with a fineness ratio of 5.5 (Fig. 6). Air volume carried by the whale at the surface ($V_{air}(0)/m_{tissue}$), was

Table 3. *Drag and buoyancy parameters calculated from least-squares fit of the model of glide forces*

Animal	Re (×10^7)	C_d (×10^{-3})	Number of glides	$V_{air}(0)$ (l 10^{-3} kg)	Number of dives	ρ_{tissue} (kg m^{-3})
sw250	2.44±0.07	2.96±0.15	46	26.3±0.9	2	1030.3
sw265	1.73±0.04	3.23±0.11	82	25.1±0.7	4	1030.4
sw275b	1.69±0.03	2.95±0.07	142	25.9±0.7	8	1030.2
sw191b	2.14±0.02	2.95±0.12	90	21.9±0.6	4	1030.3
sw209c	1.59±0.06	3.22±0.19	22	32.6±1.2	2	1028.6
Overall mean	1.92±0.36	3.06±0.15	382	26.4±3.9	20	1030.0±0.8

Values are means ± 2 S.E.M., except the overall mean, which is ± S.D.

Re, Reynold's number, C_d, drag coefficient, $V_{air}(0)$, volume of air carried by the whale from the surface, ρ_{tissue}, density of the non-air portion of the whale.

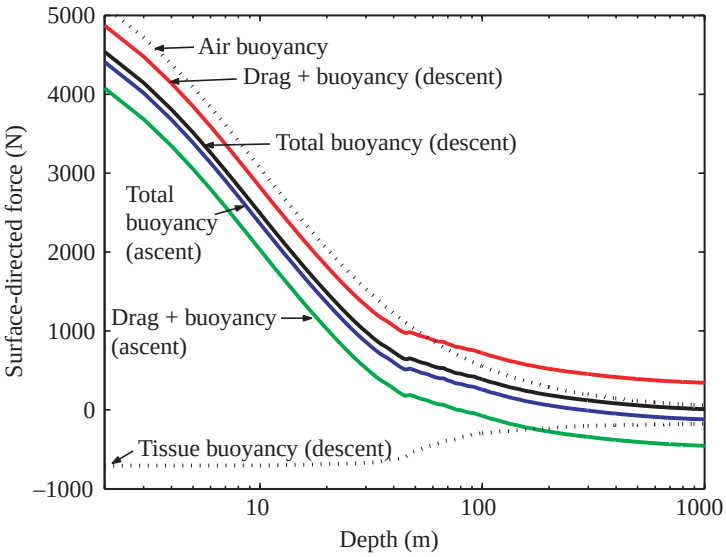

Fig. 7. Predicted drag and buoyancy forces acting on a 12.5 m sperm whale, with a mass of 25×10^3 kg, assumed to be ascending/descending at a speed of 1.5 m s^{-1}. Drag and buoyancy coefficients are based upon the model coefficients for sw275b and the temperature profile in the Mediterranean Sea. A sharp thermocline between 50 and 100 m causes a rapid decrease in negative buoyancy due to tissue density relative to seawater. After descent, the whale is at near-neutral buoyancy at 1000 m depth, which changes to ~250 m prior to ascent due to body density increases *via* cooling at depth. Positive buoyancy forces from expanding air exceed drag forces at 80 m during ascent. Thus, from this depth upward, even a whale gliding at 1.5 m s^{-1} should positively accelerate toward the surface. Note that buoyancy forces never exceed ±170 N (or half of the drag force) once the whale exceeds roughly 220 m depth.

estimated as 26.4±3.9 l kg^{-3}, and air volume carried by whales did not vary much between dives. Whale tissue density ρ_{tissue} during ascents was estimated at 1030.0±0.8 kg m^{-3}, which is 0.31%±0.07% more dense than seawater at the 40 m reference depth. Correcting for the offset between predicted and observed descent glides accelerations (Fig. 5), the density during descent would be slightly lower, 1029.3 kg m^{-3}, if the offset is due to warming at the surface (see Discussion).

To describe the drag and buoyancy forces acting on a diving sperm whale, we used the coefficients to predict drag and buoyancy forces during ascents and descents across a typical diving depth range for a 12.5 m, 25×10^3 kg whale traveling at 1.5 m s^{-1} in the Ligurian Sea (Fig. 7). Air buoyancy is quite strong near the surface (>5000 N), and decreases quickly with depth. The absolute value of the air buoyancy force becomes smaller than drag at roughly 170 m. Buoyancy imparted by sperm whale tissue is strongly affected by the increase in seawater density at depth, changing from –710 N near the surface to –180 N at depth. Combining air and tissue buoyancy after descent, the animal is within 20 N of neutral buoyancy at ~800 m depth. After cooling during bottom time, which increases tissue density by the 0.064% difference between observed and predicted accelerations during descent glides, the depth of neutral buoyancy becomes ~250 m (Fig. 7). Drag forces are predicted to be 333–334 N across all depths.

Discussion

This study provides the first detailed description of fluking behaviour of sperm whales and field estimates of their drag coefficient, air volume carried to depth, and average tissue density. The high sampling rate of the Dtag sensors allows for fine-scale measurement of animal pitch and depth, from which fluking behaviour, ascent rates and speed through the water can be obtained. Sperm whales are ideal subject animals for analysis of glides because they use them over a wide range of depths, and at different speeds (Fig. 4). By studying glide behaviour as conducted by free-ranging sperm whales, we measure the forces they actually experience in transit to, and from, deep foraging patches. Our study also benefits from the large size of the sperm whale relative to the compact Dtag, so we can discount possible influences of the small tag on total drag forces (c.f. Skrovan et al., 1999).

Our model of forces acting on sperm whales during glides (Equation 6) explained over 99% of the variability in measured accelerations during glides from five whales, and all three terms of the model had statistically significant fits at $P<0.01$ for all whales. Predictions of accelerations during descent glides correlated with observed values, with a small offset of 0.0052 m s^{-2} (Fig. 5). This offset is consistent with a decrease in animal density of 0.064% while at the surface, or a similar increase in drag during descent as opposed to ascent. Sperm whales are made up of roughly one-third blubber, which is one-third lipid. Blubber lipid contains 60% wax esters, similar in structure to that of spermaceti oil (Lockyer, 1991). For a sperm whale's density to increase by 0.064% would require the densities of these wax esters to increase by 0.9%. Spermaceti oil decreases density by ~0.5% per 1°C in the range 28–32°C (Clarke, 1978b), which is the temperature of blubber in fresh-killed sperm whales (see appendix 1 of Clarke, 1978c). Thus, even neglecting changes in the other oils in blubber, a 2°C change in blubber temperature could account for the offset between observed and predicted accelerations during descent glides. A 2°C change could occur as blubber cools at depth, and then warms when the whale is at the surface. Thermal-imaging techniques (Westgate et al., 2001) would be useful to explore temperature variations in the peripheral tissues of sperm whales, to test whether such warming does occur at the surface.

Drag coefficient, air volume and tissue density

The mean (± S.D.) estimate for passive drag coefficient C_d was 0.00306 (±0.00015) at an average Reynold's number of 1.9×10^7 ($\pm0.36\times10^7$). Because air volume is expressed per unit mass, and mass was simplified out of the tissue buoyancy term in the model, errors in the allometry analysis directly influence only the estimate for the drag term. The influence of errors on the drag estimate is somewhat reduced because animal area is in the numerator while mass is in the denominator. We refit the accelerations with a ±10% change in length (and carried this through to mass and area), which resulted in C_d changing by

±6%. Given the potential for errors in the length estimate in either direction for any one whale, the mean C_d value is the best estimate.

The drag coefficient estimates were close to those predicted for a completely turbulent spindle of fineness ratio 5.5 (Fig. 6; see Stelle et al., 2000). The sperm whale has smaller control surfaces, and may therefore be more ideally streamlined, than other odontocete cetaceans (Fish, 1993). At the high Reynold's number experienced by these large animals, flow is likely to be entirely turbulent (Vogel, 1981). In a turbulent flow regime, adaptations in shape or skin texture that delay separation of the turbulent boundary from the whale would reduce drag. Interestingly, the region of the sperm whale posterior of the dorsal fin is highly convoluted with a corrugated external surface (see fig. 18 in Berzin, 1972), which may be an adaptation to delay separation of the turbulent flow from the body. Measurements of hydrodynamic flow over this type of structure could be made to test this possibility.

Our results argue against Whitehead's conjecture (Whitehead, 2003) that sperm whales are less hydrodynamic than other large marine mammals. The largest animal for which a drag coefficient has previously been calculated from kinematic data is the killer whale, with an estimated drag coefficient of 0.0029 at Re of 3.7×10^7 (Fish, 1998), very close to our estimate for sperm whales. Based on a series of flat plates in turbulent flow, a theoretical drag coefficient of 0.0026 was estimated for a fin whale at a Reynold's number of 4.28×10^7 (Bose and Lien, 1989). Drag coefficients were calculated from glides for the Steller sea lion with an estimated C_d of 0.0056 for Re of 5.52×10^6 (Stelle et al., 2000). In the slightly smaller California sea lion, C_d was estimated at 0.0039 at a Reynold's number of 2.9×10^6 where flow is thought to be partly laminar (Feldkamp, 1987). Thus, the marine mammal species for which drag has been estimated or measured match each other fairly closely based upon the flow regime at the appropriate Reynold's number (Vogel, 1981).

Estimated volumes of air carried to depth ranged between 21.9 and 32.6 l 10^{-3} kg, with an overall mean of 26.4 l 10^{-3} kg. Variability across dives in estimate air carried to depth by each whale was quite small, with a standard deviation of 1.1 l 10^{-3} kg or less for each of the five animals (from Table 3). To our knowledge, no reliable measurements of lung volume have been made for sperm whales. However, lung mass has been measured (Omura, 1950) and is a similar percentage of body mass in sperm whales as in the bottlenosed whale *Hyperoodon ampullatus* where lung volume was measured (Clarke 1978a). Based upon these weight measurements, lung volume of sperm whales is estimated at 17.8–23.5 l 10^{-3} kg, which is close to our estimate (Clarke, 1978a). A larger lung volume is predicted from a general mammalian body size regression line that includes smaller mammals (Kooyman, 1973), but there are few data and significant variability for the larger whales. In the absence of accurate measurements of the volume of the sperm whale lung, the lung mass data summarized by Clarke (1978a) are the best information currently available. Our estimate of total air carried from the surface is roughly one-half the value of diving lung volume used by Kooyman and Ponganis (1998) to estimate total oxygen stores in the sperm whale.

The most likely function for air carried to depth by sperm whales is sound production at depth (Madsen et al., 2002), as little gas exchange is likely to occur while sperm whales are diving. While there may be gas exchange as long as the alveoli contain air, the lungs of cetaceans appear to have adaptations for rapid alveolar collapse upon diving (Kooyman, 1973). Sperm whales also have large rigid trachea and bronchi that support the collapse of alveoli (and cessation of gas exchange) upon diving (Berzin, 1972). If gases were released from tissues such as the *rete mirabile* in large quantities during ascent, we would expend to find negative residuals for the shallowest glides where gas should be released most quickly from solution (Kooyman, 1973). However, the residuals from our model were flat *versus* depth. We conclude that the impact on buoyancy due to gas release from tissues during ascent is negligible at depths greater than 38 m.

The model estimated that the density of the non-air portion of all five sperm whales was 1030 kg m^{-3}, or 0.31% denser than seawater at the reference depth of 40 m. Sperm whales killed in whaling operations are typically positively buoyant, but they are reported to sink in rare cases when air is lost due to shooting or a wound (Clarke, 1978c). Although traditional whalers preferred sperm whales because they would float upon death, Berzin (1972) reported that whalers pumped air into sperm whales to keep them from sinking and noted: '*At present sperm whales are considered to sink after death, and in fact, some of them do, primarily young animals, that have a smaller amount of fat.*' Clarke (1978c) reports a case in which a sinking whale was easily recovered on the line, suggesting only slight negative buoyancy. It therefore appears that at least some sperm whales are negatively buoyant when they have lost their air, in agreement with our findings.

Predicted forces and fluking patterns

It is important to note that all five whales for which we estimated drag coefficients, air volume carried to depth, and tissue density used the most-commonly observed pattern of fluking: steady fluking on descent and stroke-and-glide swimming on ascent. Gliding rates of these five whales (descent: 1.4%, ascent: 39.9%) were close to the overall average of all 23 sperm whales of 5.3 and 37.7%, respectively (Table 2). In contrast to these five loosely aggregated animals (mostly male) that primarily ascended without pauses at steep pitch, animals in larger social groups were more likely to show non-steep ascents with shallow ascent angles and more pauses. Several of these animals were confirmed female and were observed at the surface interacting in social groups containing small adults with a calf. These social whales appear to make use of their ascents from depth to translate their position horizontally as well as vertically, likely to maintain contact with preferred associates (Whitehead, 2003).

Based on the parameters estimated in the model (Equation 6), we are able to predict the forces acting on a

'typical' sperm whale during ascent and descent (Fig. 7) and relate these predictions to observed fluking patterns (Table 2, Fig. 3). For 'typical', we predicted forces for a 12.5 m sperm whale (mass 25×10^3 kg) with a surface area of 58.1 m^2 traveling at 1.5 m s^{-1}. Air buoyancy forces are small (+55 to +200 N) from 1000 m to 300 m. Air buoyancy then increases more rapidly to +550 N at 100 m and very quickly in the shallowest waters to +3000 N at 10 m. The buoyancy force imparted by the tissues of the sperm whale is strongly affected by the sharp decrease in density of the seawater at depth. In the Mediterranean Sea, tissue density forces for our hypothetical 12.5 m sperm whale are –710 N near the surface and decrease to –180 N at depth due to the increase in density of the displaced seawater. Note there can be a rapid change in buoyancy force as the animal passes through the thermocline (Fig. 7).

Across the depth range of a diver, the most apparent feature of these summed forces is strong positive buoyancy in the top 100 m of the water column. For an ascending whale, positive buoyancy exceeds drag and tissue buoyancy forces at roughly 80 m depth. This prediction closely matches our observations that all whales fluked strongly during the initial descent but glided during the terminal portion of the ascent. Many whales, in fact, began terminal glides at greater depths, initially decelerating and later accelerating (Fig. 3A,C).

Based on our model of forces acting on sperm whales, forces acting against descending whales are much stronger than those acting against the motion of ascending whales, at least in the top 300–400 m of the water column (Fig. 7). This overall summary of predicted forces links strongly with our finding that whales glide significantly more during ascent than descent, even though ascent speeds were higher (Table 2). The strong relationship between predicted forces and swimming gaits in our study supports the hypothesis that buoyancy affects behavioural swimming decisions in diving animals.

While there is a strong overall link between swimming behaviour and predicted forces in our study, we did find evidence of stronger positive buoyancy in four animals that made prolonged glides during ascent from depths as deep as 600 m (Table 2; Fig. 3). While no animals produced prolonged glides during descent, five whales did predominantly stroke-and-glide swimming during at least one descent and three animals (sw248a, sw249a and sw254b) glided more on descent than ascent. This suggests that some whales differ in buoyancy (both positive and negative) from the overall average observed in our 23 animals. This interpretation is most strongly supported by the finding that whales that glided more during ascent glided less during descent, and *vice versa*.

In fact, we expect significant variability in tissue buoyancy across individuals depending on the thickness and lipid content of their blubber (Beck et al., 2000; Biuw et al., 2003). Controlling for both animal size and sampling location on the body, the thickness of sperm whale blubber is highly variable across individuals (Lockyer, 1991), even those from the same social grouping (Evans et al., 2003). The buoyant middle-ventral blubber region is 9–19 cm thick in whales of 10 m length and is composed of 25–58% lipids, with typical ranges of 30% over much of the sperm whale body (Fig. 5 in Lockyer, 1991). Lipid content appears to vary independently of blubber thickness, which may further increase inter-individual variability in tissue density (Evans et al., 2003). Based upon lipid density of 850 kg m^{-3} and 10% lipid content of sperm whale tissue, a 5 cm increase (decrease) in blubber thickness will change overall tissue density to 0.16% less (0.20% more) dense than seawater. For a 25×10^3 kg animal, this would result in tissue-buoyancy forces changing by ±500 N. Adding 500 N to the model of predicted forces (Fig. 7) would result in buoyancy exceeding drag over most of the ascent depth range (creating the potential for prolonged glides during ascent), while subtracting 500 N results in negative buoyancy exceeding drag once whales reach depths greater than ~250 m (supporting more gliding in descent).

Shallow dives

We analyzed a total of 59 shallow dives to less than 65 m that lasted between 2.8 and 31.5 min. The whales swam using steady fluking or stroke-and-glide gaits in all but three of these shallow dives. While we cannot speculate why sperm whales used different swimming gaits in this context, it does suggest that choice of swimming gait may be an important behavioural option in shallow traveling dives. The efficiency with which sperm whales make use of glides appears to be relevant both for deep diving and surface travel contexts.

Based upon predictions from the glide-forces model (Fig. 7), we expect shallow-divers to be positively buoyant. At the mean shallow dive depth of 16 m, a 25×10^3 kg whale should have a positive buoyancy of more than 2000 N if it dived with a lung-full of air. While such a force could undoubtedly be overcome through hydrodynamic control during active swimming, this would entail a significant cost in swimming efficiency for the whale. Also, for three dives, one whale hung motionless in the water at less than 20 m depth for more than 10 min. This whale (sw254a) also made one prolonged glide during an ascent, suggesting that it is even more positively buoyant than the 'typical' whale modeled in Fig. 7. If 2000 N buoyancy were the only force acting on this inactive whale, it would move 20 m to the surface in less than 30 s.

Instead, we observed a clear example of buoyancy regulation by this sperm whale during shallow resting dives. After the whale had reached its maximum depth and was slowly drifting back to the surface, it released a quantity of air, which produced clearly audible bubble sounds on the tag. The ascent rate of the drifting whale slowed rapidly upon the release of the air. Occasionally, a second burst of bubbles was heard. While this behaviour was only observed in animal sw254a in the data-set reported here, it has been subsequently observed in at least two more whales tagged in the Gulf of Mexico in 2003 (P. Miller, unpublished observation). In addition to releasing bubbles, sperm whales could also regulate the volume of air they inhale before diving, as appears to occur in diving penguins (Sato et al., 2002).

Spermaceti function for buoyancy control?

It is clear from this study that buoyancy is an important factor in the ecology of sperm whales, and that sperm whales actively regulate their buoyancy, at least during shallow resting dives. Clarke (1970, 1978c) proposed that a function of the large spermaceti organ could be to regulate the buoyancy of the sperm whale at depth. The density of the spermaceti oils increase rapidly upon cooling, which could act to counter positive buoyancy that Clarke predicted for sperm whales. Lockyer (1991) suggested similar possible functions for the wax-rich lipids in the outer blubber layer of sperm whales. Several objections have been raised to this proposed function for the spermaceti organ (see review in Cranford, 1999), but few directly relevant measurements have been made. The most direct test of this hypothesis would be to measure the internal temperature of the spermaceti and other organs during dives. While this is clearly a difficult task with current technologies, indirect measures of temperature *via* sound-speed in spermaceti suggest that no significant cooling takes place during dives (Madsen et al., 2002).

The model of glide forces that we fit to ascent glide accelerations slightly underestimated the amount by which whales slow down during descent glides. This is consistent with the notion that cooling of some tissues (and increased density) may occur at depth. The scale of cooling that we observe, however, is quite small and can be fully explained by passive cooling of blubber alone. Note also that warming at the surface (and therefore lower tissue density) increases the cost of descent, while cooling at depth (which leads to higher tissue density) increases the cost of ascent. Because the blubber of sperm whales is well vascularized, heat transfer from the blood to the blubber is possible (Berzin, 1972). Clarke (1970) further suggested that warming of spermaceti oils (or blubber) through such a mechanism could increase buoyancy during ascent. To explore this possibility, we fit a second ascent model, which assumed that the whale decreased its tissue density in equilibrium with seawater temperature. This second model fit the observed acceleration data significantly worse than the glide-forces model presented in this paper and predictions of descent glide accelerations did not correlate with observed values. While we cannot rule out any warming of tissues during ascent, the glide acceleration data recorded from these five animals more strongly supports a fixed-temperature regime at least to 40 m depth, with possible warming only nearer or at the surface.

In addition, there are two aspects of our study that appear to contradict some of the important assumptions behind Clarke's hypothesis that cooling at depth may be functional for a sperm whale. First, the model fit to the glide accelerations suggests that the five sperm whales in our study are *not* neutrally buoyant (*sans* gases) at the surface, as predicted by Clarke (1970, 1978c), but have considerable negative tissue buoyancy. The sum of negative tissue and positive air buoyancy forces becomes very small when the whale is at depth (Fig. 7). The high levels of inter-individual variability in descent and ascent gliding patterns (Fig. 3) suggest that different sperm whales have varying buoyancy depending on their body condition. Fatter and more buoyant whales are the only group that would appear to benefit from extra cooling of a large organ such as the spermaceti. It seems unlikely that the massive spermaceti organ would evolve through natural selection for such a marginal benefit to those individuals that are already the most fit.

A second assumption of Clarke's hypothesis is that sperm whales have a need to remain motionless at depth to wait for prey based on reports that whales would resurface close to the location where they dived (Clarke, 1970, 1978c; Lockyer, 1991). Instead, our tag records show clearly that sperm whales actively swim during the bottom phase of their dives. This fact is borne out by steady depth-excursion throughout the bottom phase of the dive, the constant presence of acoustic flow noise, and through analysis of the accelerometer signals (see also Whitehead, 2003). Whales in different geographic locations may use different hunting strategies depending on prey type, but none of the 23 sperm whales in this study were sit-and-wait predators, all appeared to pursue prey. Therefore, any need to control buoyancy hydrostatically is reduced because the whale can overcome these forces hydrodynamically.

While more work is needed to quantify spermaceti or blubber cooling during deep dives of sperm whales, our research suggests that a special adaptation supporting additional cooling for a buoyancy function would not be particularly beneficial to sperm whales.

Thanks to the science parties on the research cruises during which these data were collected, and to Dan Engelhaupt and Amy Beier for tissue handling and sex determination. The work was conducted in collaboration with NOAA Fisheries Southeast Science Center and SACLANT Undersea Research Centre. Thanks to Tom Hurst, Alex Shorter and Jim Partan for help developing Dtag hardware and software. Funding for the research was provided under grant no. N00014-99-1-0819 from the Office of Naval Research, and Minerals Management Service Cooperative Agreements 1435-01-02-CA-85186 and NA87RJ0445. The Royal Society provided fellowship support to P.J.O.M. Thanks to Frank Fish, Dave Thompson, Mike Fedak, Peter Madsen and two anonymous reviewers for comments on the manuscript. All approaches to animals for tagging were made following the conditions of NMFS research permits 981-1575 or 981-1707. The Woods Hole Oceanographic Institution Animal Care Use Committee approved this research. This is contribution no. 11074 of the Woods Hole Oceanographic Institution.

References

Beck, C. A., Bowen, W. D. and Iverson, S. J. (2000). Seasonal changes in buoyancy and diving behaviour of adult grey seals. *J. Exp. Biol.* **203**, 2323-2330.

Berube, M. and Palsbøll, P. (1996). Identification of sex in cetaceans by multiplexing with three ZFX and ZFY specific primers. *Mol. Ecol.* **5**, 283-287.

Berzin, A. A. (1972). *The Sperm Whale.* Jerusalem: Israel Program for Scientific Translations. 394pp.

Bilo, D. and Nachtigall, W. (1980). A simple method to determine drag coefficients in aquatic animals. *J. Exp. Biol.* **87**, 357-359.

Biuw, M., McConnell, B., Bradshaw, C. J. A., Burton, H. and Fedak, M.

(2003). Blubber and buoyancy: monitoring the body condition of free-ranging seals using simple dive characteristics. *J. Exp. Biol.* **206**, 3405-3423.

Bose, N. and Lien, J. (1989). Propulsion of a fin whale (*Balaenoptera physalus*): why the fin whale is a fast swimmer. *Proc R. Soc. Lond. B* **237**, 175-200.

Clarke, M. R. (1970). Function of the spermaceti organ of the sperm whale. *Nature* **228**, 873-874.

Clarke, M. R. (1978a). Structure and proportions of the spermaceti organ in the sperm whale. *J. Mar. Biol. Assn. UK* **58**, 1-17.

Clarke, M. R. (1978b). Physical properties of spermaceti oil in the sperm whale. *J. Mar. Biol. Assn. UK* **58**, 1-17.

Clarke, M. R. (1978c). Buoyancy control as a function of the spermaceti organ in the sperm whale. *J. Mar. Biol. Assn. UK* **58**, 27-71.

Connor, R. C., Mann, J., Tyack, P. L. and Whitehead, H. (1998). Social evolution in toothed whales. *Trends Ecol. Evol.* **13**, 228-232.

Cranford, T. W. (1999). The sperm whale's nose: sexual selection on a grand scale? *Mar. Mamm. Sci.* **15**, 1133-1157.

Evans, K., Hindell, M. A. and Thiele, D. (2003). Body fat and condition in sperm whales, *Physeter macrocephalus*, from southern Australian waters. *Comp. Biochem. Phys.* **134A**, 847-862.

Fedak, M. A. and Thompson, D. (1993). Behavioural and physiological options in diving seals. *Symp. Zool. Soc. Lond.* **66**, 333-348.

Feldkamp, S. D. (1987). Swimming in the California sea lion: morphometrics, drag and energetics. *J. Exp. Biol.* **131**, 117-135.

Fish, F. E. (1993). Influence of hydrodynamic design and propulsive mode on mammalian swimming energetics. *Aust. J. Zool.* **42**, 79-101.

Fish, F. E. (1996). Transitions from drag-based to lift-based propulsion in mammalian swimming. *Am. Zool.* **36**, 628-641.

Fish, F. E. (1998). Comparative kinematics and hydrodynamics of odontocete cetaceans: morphological and ecological correlates with swimming performance. *J. Exp. Biol.* **201**, 2867-2877.

Fish, F. E. and Hui, C. A. (1991). Dolphin swimming – a review. *Mammal. Rev.* **21**, 181-195.

Fofonoff, P. and Millard, R. C. J. (1983). Algorithms for computation of fundamental properties of seawater, 1983. *UNESCO Tech. Pap. Mar. Sci.* **44**, 53.

Fujino, K. (1956). On the body proportions of the sperm whale. *Sci. Rep. Whales Res. Inst. Tokyo* **11**, 47-83.

Gordon, J. (1990). A simple photographic technique for measuring the length of whales from boats at sea. *Rep. Int. Whaling Comm.* **40**, 581-588.

Johnson, M. P. and Tyack, P. L. (2003). A digital acoustic recording tag for measuring the response of wild marine mammals to sound. *IEEE J. Ocean. Eng.* **28**, 3-12.

Kooyman, G. L. (1973). Respiratory adaptations in marine mammals. *Amer. Zool.* **13**, 457-468.

Kooyman, G. L. and Ponganis, P. J. 1998. The physiological basis of diving to depth: birds and mammals. *Annu. Rev. Physiol.* **60**, 19-32.

Lerczak, J. A. and Hobbs, R. C. (1998). Calculating sighting distances from angular readings during shipboard, aerial, and shore-based marine mammal surveys. *Mar. Mamm. Sci.* **14**, 590-599.

Lettevall, E., Richter, C., Jaquet, N., Slooten, E., Dawson, S., Whitehead, H., Christal, J. and McCall-Howard, P. (2002). Social structure and residency in aggregations of male sperm whales. *Can. J. Zool.* **80**, 1189-1196.

Lockyer, C. (1976). Body weights of some species of large whales. *J. Cons. Int. Explor. Mer.* **36**, 259-273.

Lockyer, C. (1991). Body composition of the sperm whale, *Physeter catodon*, with special reference to the possible function of fat depots. *Rit Fisk.* **12**, 1-24.

Lovvorn, J. R. and Jones, D. R. (1991). Effects of body size, body fat, and change in pressure with depth on buoyancy and costs of diving in ducks (*Aythya* sp.). *Can. J. Zool.* **69**, 2879-2887.

Madsen, P. T., Payne, R., Kristiansen, N. U., Wahlberg, M., Kerr, I. and Møhl, B. (2002). Sperm whale sound production studied with ultrasound time/depth-recording tags. *J. Exp. Biol.* **205**, 1899-1906.

Moore, M. J., Miller, C. A., Morss, M. S., Arthur, R., Lange, W. A., Prada, K. G., Marx, M. X. and Frey, E. A. (2001). Ultrasonic measurement of blubber thickness in right whales. *J. Cetacean Res. Management (Special Issue)* **2**, 301-309.

Morgan P. P. (1994). *SEAWATER: A Library of MATLAB Computational Routines for the Properties of Sea Water*. CSIRO Marine Laboratories Report 222. 29pp.

Norris, K. S. and Harvey, G. W. (1972). A theory for the function of the spermaceti organ of the sperm whale (*Physeter catodon* L.). In *NASA Special Publication* 262, *Animal Orientation and Navigation* (ed. S. R. Galler, K. Schmidt-Koenig, G. J. Jacobs and R. E. Belleville), pp. 397-417. NASA Special Publication.

Nowacek, D. P., Johnson, M. P., Tyack, P. L., Shorter, K. A., McLellan, W. and Pabst, D. A. (2001). Buoyant balaenids: the ups and downs of buoyancy in right whales. *Proc. R. Soc. Lond. B* **268**, 1811-1816.

Ogilvy, C. S. and DuBois A. B. (1982). Tail thrust of bluefish *Pomatomus saltatrix* at different buoyancies, speeds, and swimming angles. *J. Exp. Biol.* **98**, 105-117.

Omura, H. (1950). On the body weight of sperm and sei whales located in the adjacent waters of Japan. *Sci. Rep. Whales Res. Inst.* **4**, 1-13.

Pabst, D. A. (1996). Springs in swimming animals. *Am. Zool.* **36**, 723-735.

Rice, D. W. (1989). Sperm whale *Physeter macrocephalus* Linnaeus, 1758. In *Handbook of Marine Animals* (ed. S. H. Ridgway and R. Harrison), pp. 177-233. London: Academic Press.

Ridgway, S. H. (1971). Buoyancy regulation in deep diving whales. *Nature* **232**, 133-134.

Sato, K., Naito, Y., Kato, A., Niizuma, Y., Watanuki, Y., Charrassin, J. B., Bost, C.-A., Handrick, Y. and Le Maho, Y. (2002). Buoyancy and maximal diving depth in penguins: do they control inhaling air volume? *J. Exp. Biol.* **205**, 1189-1197.

Sato, K., Mitani, Y., Cameron, M. F., Siniff, D. B. and Naito, Y. (2003). Factors affecting stroking patterns and body angle in diving Weddell seals under natural conditions. *J. Exp. Biol.* **206**, 1461-1470.

Schmidt-Nielsen, K. (1997). *Animal Physiology: Adaptation and Environment*, 5th edn. Cambridge: Cambridge University Press. 612pp.

Skrovan, R. C., Williams, T. M., Berry, P. S., Moore, P. W. and Davis, R. W. (1999). The diving physiology of bottlenose dolphins (*Tursiops truncatus*) II. Biomechanics and changes in buoyancy at depth. *J. Exp. Biol.* **202**, 2479-2761.

Stelle, L. L., Blake, R. W. and Trites, A. W. (2000). Hydrodynamic drag in stellar sea lions (*Eumetopias jubatus*). *J. Exp. Biol.* **203**, 1915-1923.

Strang, G. (1991). *Introduction to Linear Algebra*. New York: Academic Press. 472pp.

Sumich, J. L. (1983). Swimming velocities, breathing patterns, and estimated costs of locomotion in migrating gray whales, *Eschrichtius robustus*. *Can. J. Zool.* **61**, 647-652.

Thompson, D., Hiby, A. R. and Fedak, M. A. (1993). How fast should I swim? Behavioural implications of diving physiology. *Symp. Zool. Soc. Lond.* **66**, 349-368.

Tucker, V. (1975). The energetic cost of moving about. *Am. Sci.* **63**, 413-419.

Vogel, S. (1981). *Life In Moving Fluids: The Physical Biology of Flow*. Princeton: Princeton University Press. 352pp.

Watkins, W. A., Daher, M. A., DiMarzio, N. A., Samuels, A., Wartzok, D., Fristrup, K. M., Howey, P. W. and Maiefski, R. R. (2002). Sperm whale dives tracked by radio tag telemetry. *Mar. Mamm. Sci.* **18**, 55-68.

Webb, P. M., Crocker, D. E., Blackwell, S. B., Costa, D. P. and LeBeouf, B. J. (1998). Effects of buoyancy on the diving behaviour of nothern elephant seals. *J. Exp. Biol.* **201**, 2349-2358.

Westgate, A. J., Pabst, D. A., McLellan, W. A., Meagher, E. M., Wells, R. S., Scott, M. D., Williams, T. A., Rommel, S. A. and Rowles, T. K. (2001). Some like it hot: measuring heat flux and temperature from wild bottlenose dolphins. *14th Biennial Conference on the Biology of Marine Mammals*, Nov 28-Dec 3, Vancouver, British Columbia.

Whitehead, H. (2003). *Sperm Whales: Social Evolution in the Ocean*. Chicago: Chicago University Press. 431pp.

Williams, T. M. (1999). The evolution of cost efficient swimming in marine mammals: limits to energetic optimization. *Phil. Trans. R. Soc. Lond. B* **354**, 193-201.

Williams, T. M., Davis, R. W., Fuiman, L. A., Francis, J., LeBeouf, B. J., Horning, M., Calambokidis, J. and Croll, D. A. (2000). Sink or swim: strategies for cost-efficient diving by marine mammals. *Science* **288**, 133-136.

Williams, T. M., Friedl, W. A., Haun, J. E. and Chun, N. K. (1993). Balancing power and speed in bottlenose dolphins (*Tursiops truncatus*). *Symp. Zool. Soc. Lond.* **66**, 383-394.

Zar, J. H. (1984). *Biostatistical Analysis*. Englewood Cliffs, NJ: Prentice-Hall.

Zimmer, W. M. X., Johnson, M. P., D'Amico, A. and Tyack, P. L. (2003). Combining data from a multisensor tag and passive sonar to determine the diving behaviour of a sperm whale (*Physeter macrocephalus*). *IEEE J. Ocean. Eng.* **28**, 13-28.